Hindawi
International Journal of Polymer Science
Volume 2020, Article ID 8866816, 12 pages
https://doi.org/10.1155/2020/8866816

Research Article

Synthesis and Optical Properties of Triphenylene-Based Donor-Donor and Donor-Acceptor Conjugated Polymers: A Comparative Study

Yong Li, Dung D. Nguyen, Kuldeep Shetye, and Zhonghua Peng

Department of Chemistry, University of Missouri-Kansas City, 5100 Rockhill Road, Kansas City, MO 64110, USA

Correspondence should be addressed to Zhonghua Peng; pengz@umkc.edu

Received 3 September 2020; Revised 20 October 2020; Accepted 24 October 2020; Published 17 November 2020

Academic Editor: Peng He

Two new conjugated polymers (**P1** and **P2**), containing a bithiophene donor unit coupled with either a triphenylene donor unit or an imide-functionalized triphenylene acceptor unit in the backbone, have been synthesized, structurally characterized, and comparatively studied by using ^{1}H NMR, FT-IR, gel permeation chromatography, differential scanning calorimetry, cyclic voltammetry, ultraviolet-visible absorption, and fluorescence spectroscopy. Both polymers are amorphous in nature and thermally stable up to 450°C. The inclusion of the imide functionalization in the triphenylene unit significantly lowered the lowest unoccupied molecular orbital energy level and thus the bandgap of the donor-acceptor polymer **P2** over the donor-donor polymer **P1**. **P1** and **P2** show very different optical properties in hexane and other solvents. **P1** shows a broad emission in hexane but vibronically structured emissions in other solvents; in contrast, **P2** exhibits a vibronically resolved emission in hexane, while exhibiting redshifted, broad, and featureless emissions in other solvents. **P1** takes a random coil conformation in good solvents like *p*-xylene, benzene, toluene, anisole, chloroform, THF, and *o*-dichlorobenzene, whereas in hexane, it may adopt a helical folding conformation. In the poor solvent DMSO, interchain aggregates dominate. **P2**, on the other hand, adopts a random coil conformation in hexane but possibly the helical folding conformation in other good solvents. The opposite conformations of the two polymers may be responsible for their opposite solvent-dependent fluorescence properties. By virtue of the very different fluorescence properties of these two polymers in nonpolar solvents such as hexane and in polar solvents, the potential of using the polymers to detect the trace amount of ethanol content that is added to gasoline has been revealed with high sensitivity.

1. Introduction

Organic semiconductors have attracted growing interest ever since the first discovery of highly conductive organic charge-transfer complexes in the 1950s [1]. They have now emerged as an appealing, commercially viable alternative to conventional inorganic semiconductor materials and have been found to have numerous cutting-edge electronic and optoelectronic applications in, for example, photovoltaic solar cells [2–7], organic light-emitting diodes [8–10], organic field effect transistors [11–13], and organic phototransistors [14–16]. The advantages of using organic molecules instead of established inorganic materials, such as silicon or gallium arsenide, include flexibility in structural modification, ease in device fabrication, and fast recovery in energy "debt" [17, 18].

Conjugated small molecules and polymers are the major types of organic semiconducting materials. Among the myriad of conjugated molecules, polycyclic aromatic compounds (PACs) have been the most extensively investigated [19–33]. In particular, triphenylene derivatives as one of the most common discotic mesogens have exhibited some unique properties attractive for various optical and/or electronic applications due to their planar geometry and extended π-delocalization [34–38]. A great number of triphenylene-based small molecules and triphenylene-containing polymers have been reported in the literature; however, conjugated

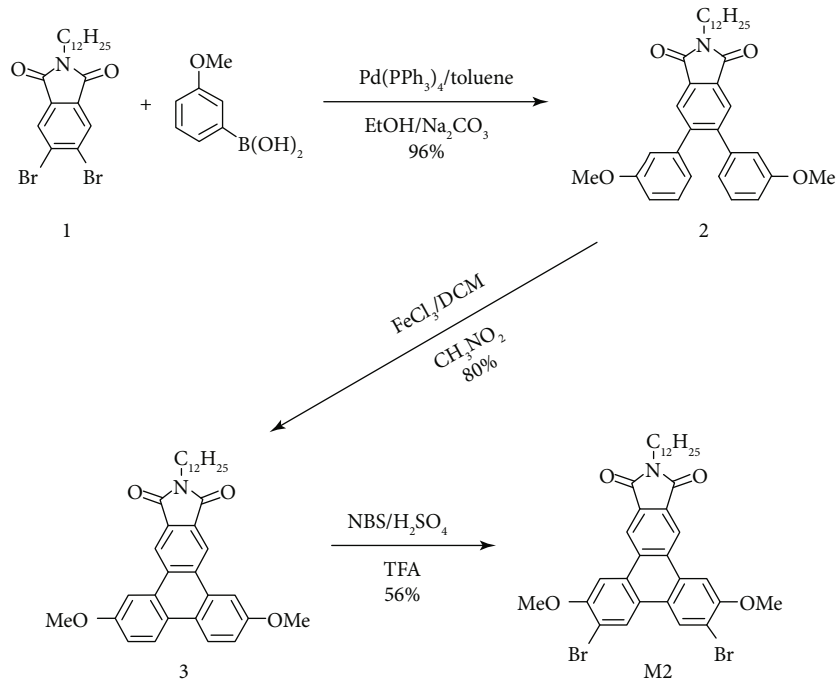

Scheme 1: Synthetic route of monomer **M2**.

polymers with triphenylene constructed as repeating units in the backbone still remain noticeably rare [39–41].

We have been interested in preparing conjugated systems containing triphenylene building blocks, including amphiphilic conjugated macrocycles, conjugated dendrimers, and conjugated polymers [41–43]. In this paper, we wish to report the synthesis and photophysical properties of two new conjugated polymers, **P1** and **P2**, containing a bithiophene donor unit coupled with either a triphenylene donor unit or an imide-functionalized triphenylene acceptor unit in the backbone. It is found that these two polymers show very different optical properties in hexane and other solvents.

2. Results and Discussion

Schemes 1 and 2 depict the synthetic routes of the imide-functionalized triphenylene-based acceptor monomer **M2** and the two triphenylene-based conjugated polymers **P1** and **P2**. The syntheses of the triphenylene-based donor monomer **M1**, the bithiophene donor comonomer **M3**, and 5,6-dibromo-2-dodecylisoindoline-1,3-dione (**1**), the starting material for the synthesis of monomer **M2**, have been reported previously [43–45].

As shown in Scheme 1, Pd-catalyzed Suzuki coupling of compound **1** with 3-methoxyphenylboronic acid gave compound **2** in excellent yields; subsequent Scholl oxidative cyclization of **2** afforded the triphenylene compound **3** in good yields; and bromination of **3** using *N*-bromosuccinimide (NBS) and catalytic amount of sulfuric acid in trifluoroacetic acid (TFA) resulted in the desired monomer **M2** in a 56% yield [46]. The desired product of each synthetic step shown in Scheme 1 can be isolated via a simple workup followed by routine purification techniques such as recrystallization, and those reactions can be easily scaled up to a multigram scale. The ^{1}H NMR spectrum of **M2** (Figure 1) showed three well-resolved, separated sharp signals (singlets) in the aromatic region at 7.98, 8.66, and 8.97 ppm, respectively, for three separated aromatic protons (g, h, and i) in the molecule, confirming the purity of the monomer.

Both polymers **P1** and **P2** were synthesized using the Stille polycondensation reaction with the Pd_2 $(dba)_3$/P(*o*-tolyl)$_3$ catalyst system. The Stille crosscoupling reaction of donor comonomer **M3** with another donor monomer **M1** yielded the donor-donor (D-D) conjugated polymer **P1** as a reddish brown solid in excellent yields (Scheme 2). The polymer was purified by dissolving in a minimum amount of good solvent like $CHCl_3$ and then precipitation in MeOH, where it had poor solubility. Similarly, the polymerization of donor comonomer **M3** and acceptor monomer **M2** was carried out following Stille coupling reaction using THF as the solvent for about 40 h to yield the donor-acceptor (D-A) conjugated polymer **P2** in excellent yields (Scheme 2). The synthesized polymer **P2** was isolated by repeated dissolution-precipitation-separation steps, giving **P2** as a dark red solid.

Introducing the multiple long dodecyl chains into the structure improves the solubility of the polymers **P1** and **P2** in most of the organic solvents. **P1** is soluble in nonpolar solvent like hexane, while **P2** is only partially soluble in hexane. Both **P1** and **P2** have good solubility in solvents like *p*-xylene, benzene, toluene, anisole, chloroform, tetrahydrofuran (THF), and *o*-dichlorobenzene (ODCB) but very poor solubility in dimethylformamide (DMF). These two polymers are completely insoluble in dimethyl sulfoxide (DMSO) at room temperature.

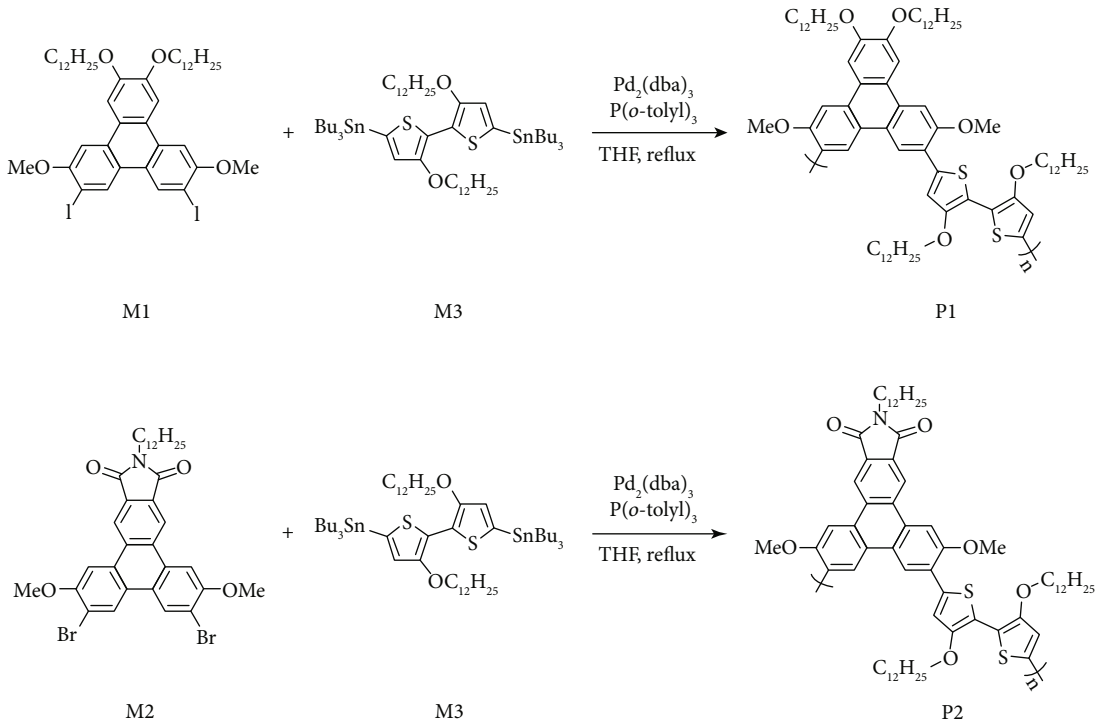

Scheme 2: Synthesis of polymers **P1** and **P2**.

Figure 2 shows the ^{1}H NMR spectra of the two polymers **P1** and **P2** in $CDCl_3$. As can be seen, the characteristic sharp signals in the aromatic region and those for the methoxy, dodecyloxy, and/or N-dodecyl protons in monomers (Figure 1 and Figure S1) are all replaced by broad signals in polymers, presumably due to interpolymer aggregation. The broadening of these peaks, as well as, for example, some downfield shift for protons labeled as h and g in Figure 2, in both polymers **P1** and **P2** indicates the clear distinction from their monomers and suggests that there is much stronger intermolecular aggregation in the polymers. The signal labeled as k′ is likely the end group signal.

Figure 3 shows the FT-IR spectra of **P1** and **P2**. There are several characteristic vibrations due to the presence of imide functionalization in **P2**. The strong band at ~1707 cm^{-1} is assigned to the symmetrical stretching vibration of the C=O bond in the imide-functionalized triphenylene units, while the band at ~1765 cm^{-1} is attributed to C=O asymmetrical stretching. The band at ~1388 cm^{-1} corresponds to the C-N stretching, and the band around 747 cm^{-1} is designated to the C=O bending from the imide groups. These vibrations were absent in **P1** as it does not contain imide groups in the structure.

Polymers **P1** and **P2** were characterized by gel permeation chromatography (GPC) to estimate the molecular weights using THF as an eluent and polystyrene as the standard (Figure S6). The number average molecular weight (M_n) of polymer **P1** was found to be 6.23 kDa, while the weight average molecular weight (M_w) was 7.40 kDa. For polymer **P2**, M_n and M_w were estimated to be 4.40 and 5.09 kDa, respectively. Both polymers have narrow polydispersity indices (PDI) (1.19 and 1.16 for **P1** and **P2**, respectively). It is worth noting that the calculated molecular weights based on polystyrene standards may not be accurate for conjugated polymers **P1** and **P2** especially when considering the potentially folding conformations of the polymers.

The thermal properties of the two polymers were investigated by using differential scanning calorimetry (DSC) in N_2 with a heating and cooling rate of 10°C min^{-1}. As can be seen from Figure 4, both polymers happened to be amorphous in nature with no obvious thermal transitions and they are both thermally stable up to 450°C.

The electrochemical properties of the two triphenylene-containing conjugated polymers were studied as thin films using cyclic voltammetry (CV) measurements. For polymer **P1**, one irreversible reduction wave was observed during the cathodic scan, and three irreversible oxidation waves were shown during the anodic scan as seen in Figure 5. In the case of polymer **P2**, three reversible reduction waves were observed during the cathodic scan, and two semireversible oxidation waves were seen during the anodic scan. By making use of the first oxidation onset potential during the anodic scan (E_{ox}^{onset} = 0.13 V for **P1** and 0.14 V for **P2**) and the first reduction onset potential in the cathodic scan (E_{red}^{onset} = −2.24 V for **P1** and−1.28 V for **P2**), the highest occupied molecular orbital (HOMO) and lowest unoccupied molecular orbital (LUMO) energy levels of the polymers **P1** and **P2** were estimated to be −4.92/−2.56 and −4.94/−3.52 eV, respectively. In a D-A conjugated polymer, the HOMO energy level is controlled by the D unit, while the LUMO energy level is controlled by the A unit. In the cases of both polymers **P1** and **P2**, their donor comonomers are the same, and their HOMO

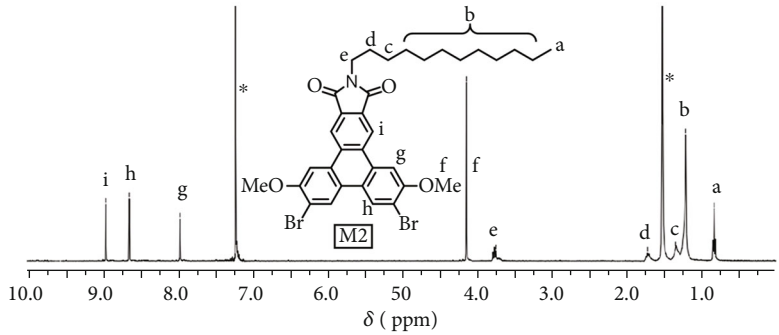

Figure 1: ^{1}H NMR spectrum of monomer **M2** in $CDCl_3$ (signals labeled with "∗" are solvent peaks).

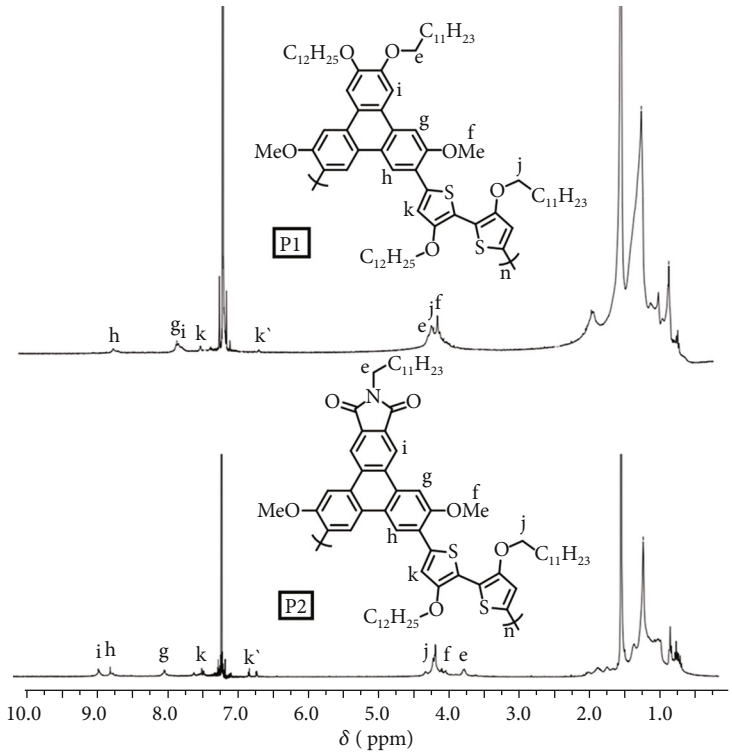

Figure 2: ^{1}H NMR spectra of the two polymers **P1** and **P2**.

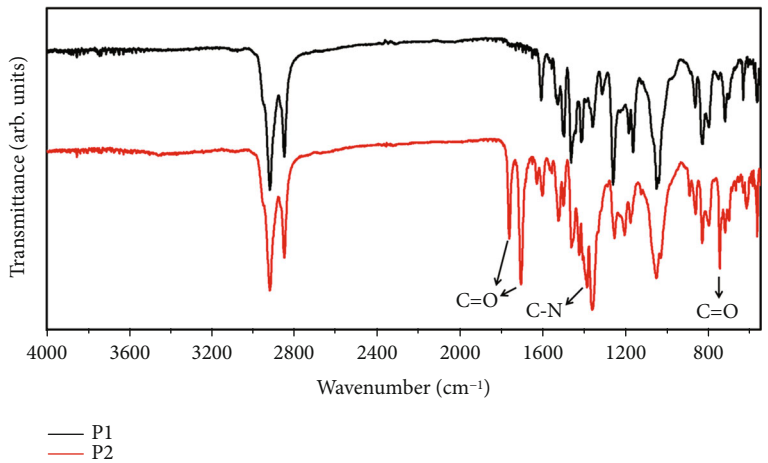

Figure 3: FT-IR spectra of polymers **P1** and **P2**.

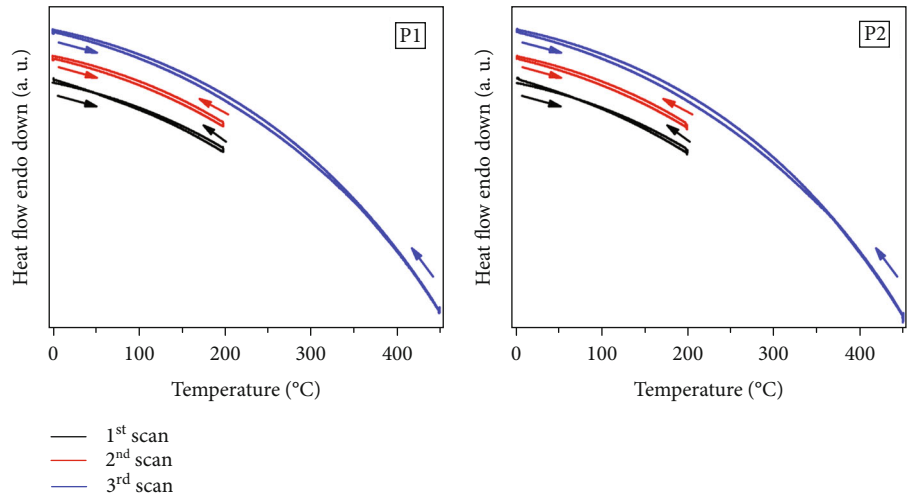

Figure 4: DSC thermograms of the polymers **P1** and **P2** with a heating and cooling rate of 10°C min^{-1}. Note that the DSC thermograms of successive scans were offset for clarity.

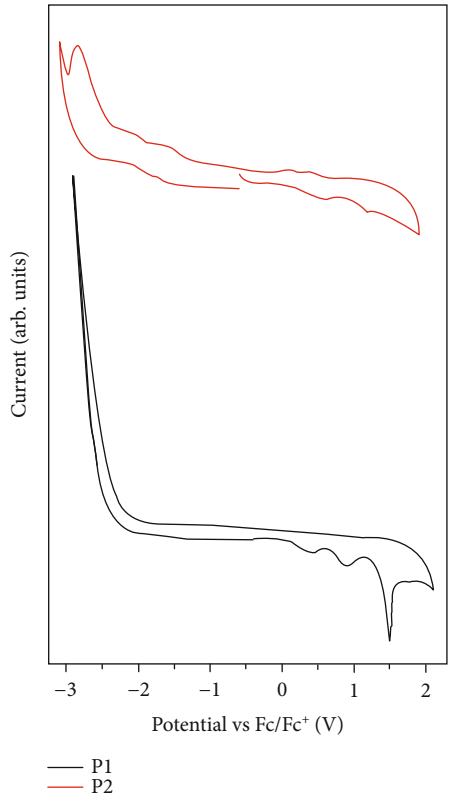

Figure 5: Cyclic voltammograms of the polymer thin films. Note that these curves are both first scans of cyclic voltammetry.

levels are very close to each other, while their LUMO levels are very different. The LUMO energy level in the case of polymer **P2** was lowered substantially due to the presence of imide functionalization, and that in turn lowered the effective bandgap. The bandgaps of polymers **P1** and **P2** were found to be 2.36 and 1.42 eV, respectively.

Figure 6 shows the absorption spectra of the polymers **P1** and **P2** as dilute solutions in different solvents with their absorption maxima compiled in Table 1. As can be seen, polymer **P1** exhibit one broad absorption band centered at 436~440 nm in the visible region in good solvents like *p*-xylene, benzene, toluene, anisole, chloroform, THF, and ODCB. In hexane and the two solvents (DMF and DMSO) in which both polymers exhibit poor solubility, one notices a prominent shoulder peak around 500 nm besides the major absorption band. There is about 10 nm redshift for the maximum absorption wavelength in the visible range for **P1** in DMSO as compared to the other solvents. In hexane and DMSO, **P1** also shows an absorption tail longer than that in the other solvents, extending to ~750 nm. The absorption shoulder/long tail in DMSO is likely due to the stronger interchain aggregation and/or interchain π-π overlap resulting from the poor solubility of **P1**. In hexane, however, **P1** exhibits good solubility. The redshifted shoulder band and the long tail are attributed likely to an intrachain π-π stacking interaction. In other words, **P1** in hexane likely adopts a folding conformation, which is consistent with its fluorescence properties discussed later. In the case of polymer **P2**, there is only one broad absorption band in the visible region in the same variety of solvents. A redshift of 18 nm is observed for the absorption maximum in the visible range when the solvent is changed from hexane to DMSO. An absorption tail extending to longer wavelengths is observed for **P2** in all three poor solvents (hexane, DMF, and DMSO).

These two polymers are moderately to weakly fluorescent in different organic solvents, and their fluorescence behaviors were found to be strongly dependent on the type of the organic solvents. Figure 7 shows the absorbance-corrected fluorescence emission spectra of polymers **P1** and **P2** as dilute solutions in different solvents with their emission maxima and fluorescence quantum yields summarized in Table 2 and detailed excitation/emission spectra illustrated in Figures S2 and S3 in the supporting information. In all good solvents studied with the exception of hexane, polymer **P1** exhibits very similar vibronically structured fluorescence emissions, indicating that **P1** adopts a random coil conformation in those solvents. In the poor solvent

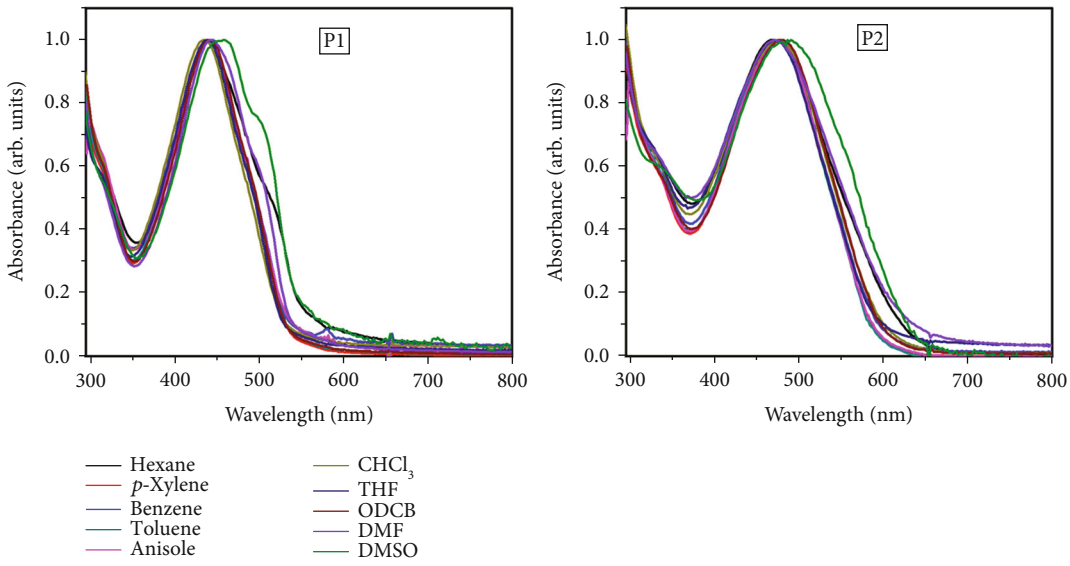

Figure 6: UV-Vis absorption spectra of **P1** and **P2** as dilute solutions in different solvents. Note that **P2** has poor solubility in hexane, and the upper, clear portion of a saturated **P2** solution in hexane was collected and used for measurement. Also, note that due to the very poor solubility of **P1** and **P2** in DMF and the insolubility of **P1** and **P2** in DMSO, these solutions were prepared by adding a very small amount of concentrated $CHCl_3$ stock solution of **P1** or **P2** to respective solvents.

Table 1: Absorption maxima of **P1** and **P2** as dilute solutions in different solvents.

Polymer	λ_{max}^{abs} (nm)									
	Hexane (1.9)	*p*-Xylene (2.268)	Benzene (2.27)	Toluene (2.38)	Anisole (4.33)	$CHCl_3$ (4.81)	THF (7.58)	ODCB (9.93)	DMF (36.7)	DMSO (46.7)
P1	440	440	438	440	442	436	438	440	442[b]	458[b]
P2	468[a]	476	474	478	476	474	472	482	472[b]	486[b]

[a]**P2** has poor solubility in hexane, and the upper, clear portion of a saturated **P2** solution in hexane was collected and used for measurement. [b]Due to the very poor solubility of **P1** and **P2** in DMF and the insolubility of **P1** and **P2** in DMSO, these solutions were prepared by adding a very small amount of concentrated $CHCl_3$ stock solution of **P1** or **P2** to respective solvents. The numbers in brackets are the dielectric constants of the solvents.

DMSO, **P1** shows extremely weak fluorescence barely discernable by the instrument (Figure S2). The weak emission is broad with a significantly redshifted emission maximum λ_{max} at 585 nm. The weak, broad, and significantly redshifted emission of **P1** in DMSO is attributed to the strong interchain π-π stacking interaction of **P1** in poor solvent. In hexane, the emission of **P1** is again broad and lacks vibronic bands. However, the maximum emission wavelength (λ_{max} 543 nm) in hexane is higher than those in the other good solvents but lower than that in DMSO, indicating that **P1** in hexane does not adopt a random coil conformation as in other good solvents nor exist as interchain aggregates as it does in DMSO. As alluded to earlier, we suggest that **P1** in hexane adopts a helical folding conformation driven by intrachain π-π stacking interactions that gave rise to its unique fluorescence emissions. The strong interdigitation of long alkyl side chains in **P1** with the solvent hexane likely plays a significant role in driving **P1** helical folding since folding exposes long alkyl chains towards the solvent.

Interestingly, the fluorescence emissions of **P2** show solvent dependence that is almost opposite to that of **P1**. As can be seen in Figure 7, **P2** in all solvents except for hexane shows one broad structureless emission. It seems that, contrary to **P1**, **P2** adopts a folding conformation in all good solvents studied. The stronger folding tendency of **P2** is likely due to the stronger π-π stacking interaction among the imide-functionalized triphenylene units. The emission of **P2** in hexane, however, is blueshifted and vibronically structured. The emission intensity of **P2** is significantly lower in hexane than in the other three nonpolar solvents (*p*-xylene, benzene, and toluene) but higher than in the rest of the solvents which all happen to have higher dielectric constants than hexane. The blueshifted and vibronically structured emission may indicate a random coil conformation of **P2** in hexane. The fluorescence emission spectra of **P2** as dilute solutions in mixed hexane/toluene solvents with varied volume ratios were studied and are shown in Figure 8. Note that the same amount of saturated hexane stock solution was used for the preparation of all these solutions, and the overall concentration of **P2** was kept constant. As can be seen from Figure 8, when the volume percentage of toluene increases from 0 to 80% in a gradual manner, **P2** shows a clear and continuous transition from the vibronically resolved emission in pure hexane with maximum emission wavelength at 519 nm towards a redshifted, broad, and featureless emission

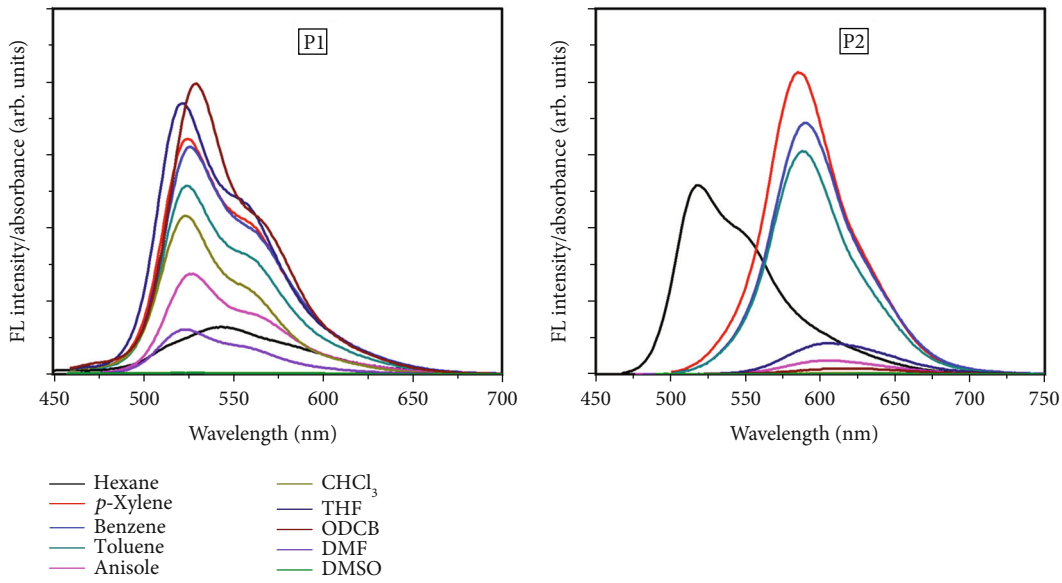

Figure 7: Absorbance-corrected fluorescence emission (excited at the corresponding absorption maximum) spectra of **P1** and **P2** as very dilute solutions (maximum absorbance: ca. 0.1) in different solvents. Note that **P2** has poor solubility in hexane, and the upper, clear portion of a saturated **P2** solution in hexane was collected and diluted for measurement. Also, note that due to the very poor solubility of **P1** and **P2** in DMF and the insolubility of **P1** and **P2** in DMSO, these solutions were prepared by adding a very small amount of concentrated $CHCl_3$ stock solution of **P1** or **P2** to respective solvents.

Table 2: Emission maxima (excited at the corresponding absorption maximum) and fluorescence quantum yields of **P1** and **P2** as very dilute solutions (maximum absorbance: ca. 0.1) in different solvents.

Solvent	P1		P2	
	λ_{max}^{fl} (nm)	φ^a	λ_{max}^{fl} (nm)	φ^a
Hexane (1.9)	543	0.021	519[c]	0.070[c]
p-Xylene (2.268)	525	0.093	585	0.121
Benzene (2.27)	526	0.091	590	0.103
Toluene (2.38)	524	0.073	588	0.090
Anisole (4.33)	526	0.039	604	0.007
$CHCl_3$ (4.81)	524	0.052	611	<0.001
THF (7.58)	522	0.092	606	0.013
ODCB (9.93)	530	0.112	612	0.004
DMF (36.7)	524[b]	0.015[b]	—[b]	<0.001[b]
DMSO (46.7)	585[b]	0.001[b]	647[b]	<0.001[b]

[a]Fluorescence quantum yield. [b]Due to the very poor solubility of **P1** and **P2** in DMF and insolubility of **P1** and **P2** in DMSO, these solutions were prepared by adding a very small amount of concentrated $CHCl_3$ stock solution of **P1** or **P2** to respective solvents. [c]**P2** has poor solubility in hexane, and the upper, clear portion of a saturated **P2** solution in hexane was collected and diluted for measurement. The numbers in brackets are the dielectric constants of the solvents.

centered at ~580 nm in the mixed solvent containing 20% hexane and 80% toluene, the latter of which is similar to the one in pure toluene solvent (Figure 7). This result indicates that the different fluorescent properties of **P2** in hexane from those in the other solvents are not due to molecular weight difference of dissolved **P2** polymers but rather the result of **P2** polymers taking a different conformation (random coil instead of folded helices).

Noticing the varied fluorescence intensities and shifting of emission bands of **P1** and **P2** in the different solvents, we further compared the absorbance-corrected, integrated fluorescence intensity and maximum emission wavelength of **P1** and **P2** as very dilute solutions as a function of the dielectric constant of the solvent (Figure 9 and Figure S4). Due to the very different fluorescence behavior in hexane and the extremely weak fluorescence intensities in DMF and DMSO, these three solvents are excluded from the plots in Figure 9. For **P1**, when the polarity of the solvent increases, its fluorescence intensity first decreases and then increases, while no clear trend can be seen for its emission maximum. For **P2**, when the polarity of the solvent increases, its fluorescence intensity generally decreases, and its emission maximum shifts to longer wavelength with small fluctuations. **P2** is highly fluorescent in the three good nonpolar solvents (benzene, *p*-xylene, and toluene). The fluorescence intensity drops significantly when the dielectric constant of the solvent is changed slightly from toluene to anisole, accompanied by a sizable redshift in emission wavelengths.

It is interesting to note the significant differences in the solvent-dependent emission properties of polymers **P1** and **P2** in chloroform and hexane. For **P1**, the polymer is more fluorescent in $CHCl_3$ and the emission λ_{max} is blueshifted by 19 nm compared to that in hexane. For **P2**, the observation is exactly opposite: polymer **P2** has significantly less fluorescence emission in chloroform and the emission λ_{max} in chloroform is significantly redshifted by 92 nm compared to that in hexane. In order to further understand the effect of solvent composition on the emission of the polymers, a

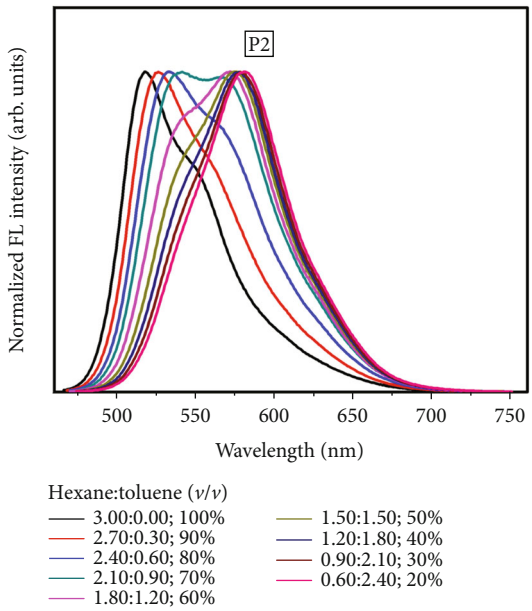

Figure 8: Normalized fluorescence emission (excited at the corresponding absorption maximum) spectra of **P2** as dilute solutions in pure hexane and mixed hexane/toluene solvents. Note that **P2** has poor solubility in hexane, and the upper, clear portion of a saturated **P2** solution in hexane was collected and used as the stock solution. The same amount of stock solution was used for the preparation of the solutions, and the overall concentration of **P2** was kept constant.

$CHCl_3$ solution of **P1** was used as a stock solution and the concentration was kept constant, and the hexane content was continuously increased in the mixed solvent; for **P2**, a hexane solution was adopted as the stock solution, and the $CHCl_3$ content continuously increased in the mixed solvent. Results are compiled in Figure 10 and Figure S5. As can be observed, for **P1**, there was a continuous decrease in the fluorescence quantum yield, or a fluorescence quenching effect, as the $CHCl_3$ content decreased, but there was not much shift in the emission wavelength. For **P2**, as the $CHCl_3$ content increased, there were a clear redshift in the emission wavelength and a decrease in the fluorescence intensity. The drastic changes in the emission spectra indicate that the polymers adopt different conformations in these two solvents.

As mentioned earlier, **P1** takes a random coil conformation in good solvents like *p*-xylene, benzene, toluene, anisole, chloroform, THF, and ODCB, whereas in hexane, it may adopt a helical folding conformation. In the poor solvent DMSO, interchain aggregates dominate. **P2**, on the other hand, adopts a random coil conformation in hexane but possibly the helical folding conformation in other good solvents. The opposite conformations of the two polymers may be responsible for their opposite solvent-dependent fluorescence properties. Although the above interpretations are logical, future effort is needed for providing direct evidence to support the folding hypothesis of these polymers.

Ethanol (normally 10 vol%) is frequently added to gasoline to improve combustion. Seeing that **P1** and **P2** have very different fluorescence properties in hexane and polar solvents, we explored whether these polymers can be used as fluorescence sensors to detect the ethanol content that is added to gasoline. Hexane was used to represent gasoline in the present study. Figure 11 shows the absorbance-corrected fluorescence emission spectra of **P1** and **P2** as dilute solutions in mixed hexane/EtOH solvent of different volume ratios. Figure 12 shows their integrated fluorescence intensity plots as a function of volume percentage of EtOH. As can be seen, both polymers respond to the ethanol content changes but to a different extent. The fluorescence intensity of **P1** dropped slowly until the ethanol percentage reached 50% and then dropped much faster passing 60%. In contrast, polymer **P2** is ultrasensitive to the trace amount of ethanol content added, with its fluorescence intensity experiencing a fast decrease when the ethanol volume percentage increases. When 10 vol% of ethanol is added to hexane, the fluorescence intensity dropped to only 3.5% of its original value in pure hexane.

In summary, we have successfully synthesized two triphenylene-based conjugated polymers: **P1** containing a triphenylene donor unit and a bithiophene donor unit and **P2** containing an imide-functionalized triphenylene acceptor unit and the same bithiophene donor unit. The structures of the D-D and D-A polymers were characterized by ^{1}H NMR and FT-IR, and their molecular weights were determined by gel permeation chromatography. Both polymers are amorphous in nature and thermally stable up to 450°C. The inclusion of the imide functionalization in the triphenylene unit significantly lowered the LUMO energy level and thus the bandgap of the D-A polymer **P2** over the D-D polymer **P1**. **P1** and **P2** show very different optical properties in hexane and other solvents, indicating that the polymers adopt different conformations in the solvents. **P1** shows a broad emission in hexane but vibronically structured emissions in other solvents; in contrast, **P2** exhibits a vibronically resolved emission in hexane, while exhibiting redshifted, broad, and featureless emissions in other solvents. It is likely that **P1** takes a random coil conformation in good solvents like *p*-xylene, benzene, toluene, anisole, chloroform, THF, and ODCB, whereas in hexane, it takes an intrachain folding conformation. In the nonpolar hexane solvent, **P2** adopts a random coil conformation with blueshifted monomeric fluorescence emissions, while in other good solvents, it adopts the intrachain folding conformation with redshifted, featureless emissions. By virtue of the very different fluorescence properties of these two polymers in hexane and polar solvents, the potential of using the polymers to detect the trace amount of ethanol content that is added to gasoline has also been revealed with high sensitivity.

3. Experimental Section

Dichloromethane (DCM) was distilled from CaH_2 immediately before use. THF was purified by distillation over sodium/benzophenone prior to use. Acetonitrile was freshly distilled from CaH_2 under nitrogen. Unless otherwise stated, all other chemicals were used as received from Sigma-Aldrich or Fisher Scientific without further purification. All reactions were carried out under nitrogen using the standard Schlenk

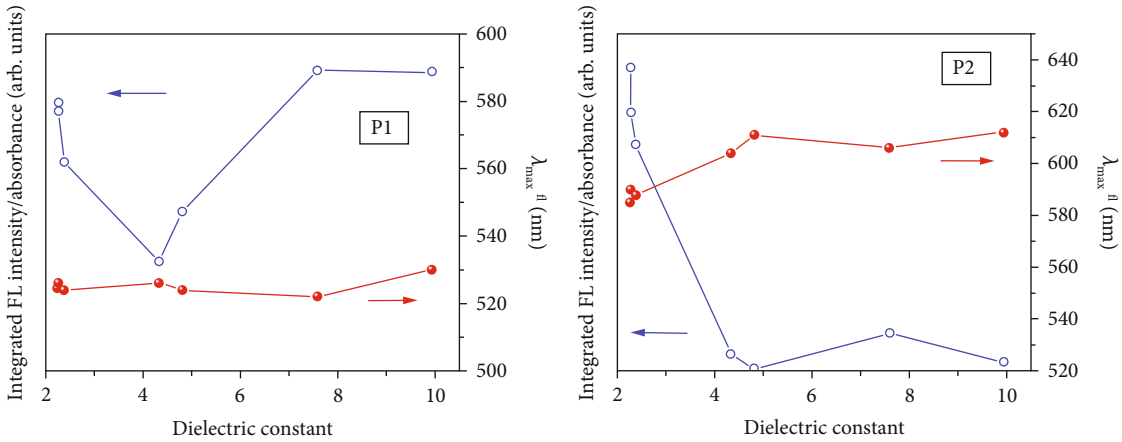

Figure 9: Plots of absorbance-corrected, integrated fluorescence intensity (excited at the corresponding absorption maximum) and maximum emission wavelength of **P1** and **P2** as very dilute solutions (maximum absorbance: ca. 0.1) in different solvents as a function of the dielectric constant of the solvent. Note that hexane, DMF, and DMSO are excluded.

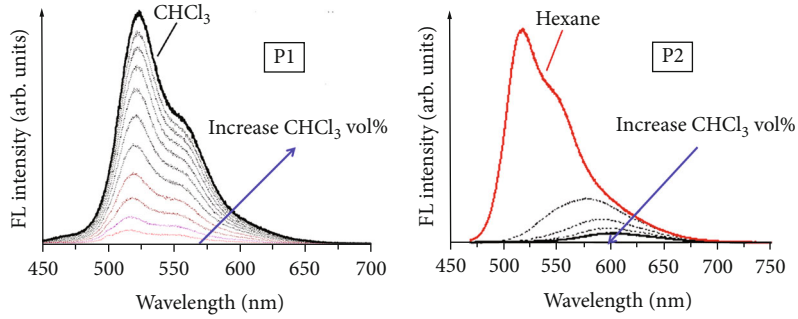

Figure 10: Absorbance-corrected fluorescence emission (excited at the corresponding absorption maximum) spectra of **P1** and **P2** as dilute solutions in hexane, $CHCl_3$, or mixed hexane/$CHCl_3$ solvent. Note that **P2** has poor solubility in hexane, and the upper, clear portion of a saturated **P2** solution in hexane was collected and used as the stock solution. See Figure S5 for more detailed studies on **P2**.

techniques. ^{1}H and ^{13}C NMR spectra were collected on a Varian Inova 400 MHz NMR spectrometer in deuterated solvents. Chemical shifts are internally referenced to the residual solvent resonance signal. DSC thermograms were recorded on a PerkinElmer DSC 8000 differential scanning calorimeter. FT-IR spectra were recorded with a Shimadzu IRAffinity-1 Fourier transform infrared spectrophotometer. UV-visible absorption spectra were measured with a Hewlett-Packard 8452A diode array spectrophotometer. Fluorescence spectra were recorded on a Shimadzu RF-5301PC spectrofluorophotometer. The GPC measurements were performed at 30°C on a Tosoh EcoSEC HLC-8320GPC system equipped with a differential refractometer, a UV detector, and a styragel column with THF as the eluent. The calibration curve was determined by the use of a set of four polystyrene standards (from 474 to 549000).

CV measurements of the polymer thin films were carried out under argon using a BAS Epsilon EC electrochemical station employing a Pt working electrode, a silver wire reference electrode, and a Pt wire counter electrode. A 0.1 M $[Bu_4N]PF_6$ solution in acetonitrile was used as the supporting electrolyte, and the scan rate was 20 mVs^{-1}. Fc/Fc^+ was used as the reference and assigned an absolute energy of −4.80 eV versus vacuum. The HOMO and the LUMO energy levels were calculated by HOMO $= -(E_{ox}{}^{onset} + 4.80)$ (eV) and LUMO $= -(E_{red}{}^{onset} + 4.80)$ (eV), respectively.

Monomer **M1** and comonomer **M3**, as well as compound **1**, were synthesized following previously reported procedures [43–45].

3.1. Compound **2**. Compound **1** (0.50 g, 1.06 mmol) and 3-methoxyphenylboronic acid (0.39 g, 2.53 mmol) were added to a Schlenk flask, and the mixture was subjected to three cycles of pumping and purging with N_2. Toluene (50 mL) and ethanol (20 mL) were then added to the flask, followed by the addition of tetrakis(triphenylphosphine)palladium (0) (0.06 g, 0.05 mmol) and sodium bicarbonate (0.67 g, 6.33 mmol). The reaction mixture was stirred under reflux for 16 h. It was then cooled to room temperature and neutralized with 10% HCl. It was then washed with deionized (DI) water, and the aqueous layer was extracted with DCM (3 × 30 mL). The organic layers were combined and dried over magnesium sulfate. The solvent was removed to give thick yellow liquid as the crude product. It was purified by column chromatography on a silica gel with ethyl acetate/hexane (30/70) as the eluent, affording **2** as a yellow solid (0.54 g, 1.02 mmol, 96%). ^{1}H NMR (400 MHz, $CDCl_3$, δ (ppm)): 9.02 (s, 2H, Ar-H), 8.51 (dd, J = 8 Hz, 2H, Ar-H), 8.04 (s, 2H, Ar-

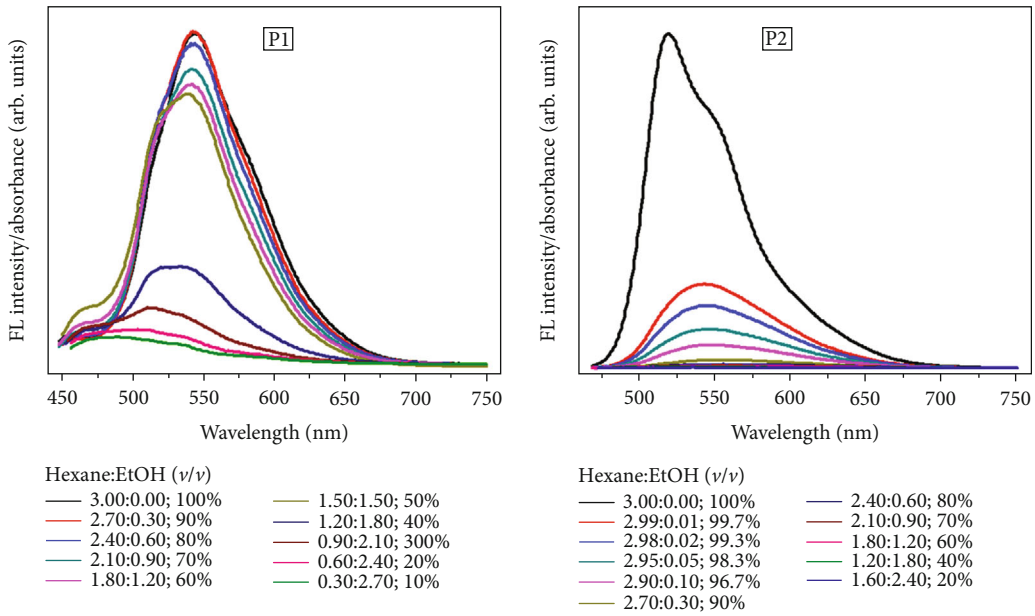

Figure 11: Absorbance-corrected fluorescence emission (excited at the corresponding absorption maximum) spectra of **P1** and **P2** as dilute solutions in mixed hexane/EtOH solvent of different volume ratios. Note that **P2** has poor solubility in hexane, and the upper, clear portion of a saturated **P2** solution in hexane was collected and used as the stock solution.

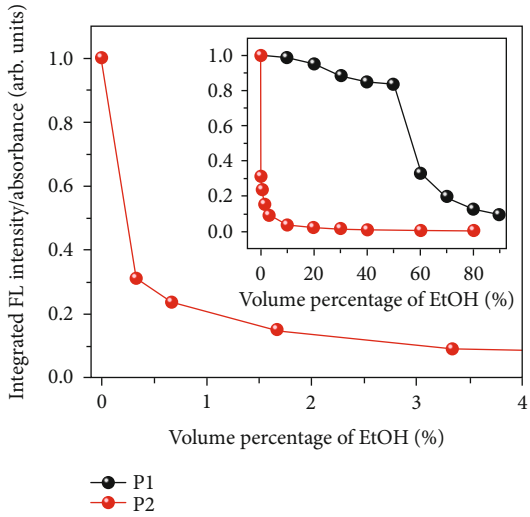

Figure 12: Plots of normalized, absorbance-corrected, integrated fluorescence intensity (excited at the corresponding absorption maximum) of **P1** and **P2** as dilute solutions in mixed hexane/EtOH solvent as a function of volume percentage of EtOH. Note that **P2** has poor solubility in hexane, and the upper, clear portion of a saturated **P2** solution in hexane was collected and used as the stock solution.

H), 7.37 (d, $J = 4$ Hz, 2H, Ar-H), 7.35 (d, 2H, Ar-H), 4.05 (s, 6H, -O-CH_3), 3.77 (t, $J = 8$ Hz, 2H, -N-CH_2-), 1.73 (m, 2H, -CH_2-), 1.23 (m, 18H, -CH_2-), 0.84 (t, $J = 6$ Hz, 3H, -CH_3).

3.2. Compound **3**. To a Schlenk flask was added compound **2** (0.90 g, 1.71 mmol), and the flask was subjected to three cycles of pumping and purging with N_2. To this flask was added freshly distilled DCM (90 mL), followed by the addition of iron (III) chloride (1.38 g, 8.55 mmol) in nitromethane (20 mL). The resulting reaction mixture was stirred at room temperature for approximately 20 min. Methanol (60 mL) was then added, and the mixture was stirred for another 1 h. It was then poured into DI water and was extracted with DCM. The organic layers were combined and dried over $MgSO_4$. It was passed through a filtration column, and the solvent was evaporated to give the orange crude product. It was then recrystallized from DCM/methanol to give compound **3** as yellow solids (0.72 g, 1.37 mmol, 80%). ^{1}H NMR (400 MHz, $CDCl_3$, δ (ppm)): 9.42 (s, 2H, Ar-H), 8.48 (d, $J = 12$ Hz, 2H, Ar-H), 8.04 (s, 2H, Ar-H), 7.46 (dd, $J = 8$ Hz, 2H, Ar-H), 4.05 (s, 6H, -O-CH_3), 3.77 (t, $J = 8$ Hz, 2H, -N-CH_2-), 1.73 (m, 2H, -CH_2-), 1.22 (m, 18H, -CH_2-), 0.84 (t, $J = 6$ Hz, 3H, -CH_3). ^{13}C NMR (400 MHz, $CDCl_3$, δ (ppm)): 168.7, 158.7, 133.9, 129.5, 129.2, 124.9, 124.8, 119.0, 118.7, 105.6, 55.9, 38.6, 32.1, 29.9, 29.8, 29.6, 29.5, 28.9, 27.2, 22.9, 14.4.

3.3. Monomer **M2**. To a RB flask containing compound **3** (0.50 g, 0.95 mmol) and TFA (22.5 mL) was added conc. H_2SO_4 (5 mL) dropwise. NBS (0.42 g, 2.38 mmol) was then added to the above solution to yield a dark red colored soln. The resulting mixture was stirred at room temperature overnight and was then diluted with DI water. The solution was extracted with DCM. The organic layers were collected and dried over $MgSO_4$. The solvent was evaporated to give reddish solids as the crude product which was purified by recrystallization from DCM/CH_3OH to yield monomer **M2** as a pale yellow solid (0.36 g, 0.53 mmol, 56%). ^{1}H NMR (400 MHz, $CDCl_3$, δ (ppm)): 8.97 (s, 2H, Ar-H), 8.66 (s, 2H, Ar-H), 7.98 (s, 2H, Ar-H), 4.16 (s, 6H, -O-CH_3), 3.76 (t, $J = 8$ Hz, 2H, -N-CH_2-

), 1.73 (m, 2H, -CH_2-), 1.22 (m, 18H, -CH_2-), 0.84 (t, J = 8 Hz, 3H, -CH_3).

3.4. Polymer **P1**. To a two-neck Schlenk flask under argon protection were added monomer **M1** (85.7 mg, 0.09 mmol) and comonomer **M3** (105 mg, 0.09 mmol), tris(dibenzylideneacetone)dipalladium(0) (4.3 mg, 0.005 mmol), and tri(*o*-tolyl)phosphine (11.5 mg, 0.04 mmol). The flask was subjected to three cycles of pumping and purging with argon. To this flask was added freshly distilled THF (5 mL), and the reaction mixture was refluxed at 80°C for 60 h. After cooling to room temperature, the reaction mixture was poured into a solvent mixture containing methanol (45 mL) and 12 N HCl (5 mL). It was stirred for an additional 3 h. The precipitate was collected by centrifugation and was poured into solvent mixture containing methanol (45 mL) and chloroform (5 mL). It was again stirred for 3 h, and the precipitate was collected by centrifugation and dried under reduced pressure to give the polymer as reddish brown solids (109 mg, 0.09 mmol, 95%). ^{1}H NMR (400 MHz, $CDCl_3$, δ (ppm)): 8.81 (br, 2H, Ar-H), 7.90 (br, 2H, Ar-H), 6.75 (br, 2H, thiophene H's), 4.0-4.4 (br, 14H, -OCH_2-, -OCH_2- [on thiophene], -OCH_3), 1.97 (br, 8H, -CH_2-), 1.26 (br, 72H, -CH_2-), 1.10-0.99 (br, 6H, -CH_3), 0.93-0.82 (br, 6H, -CH_3). Molecular weights from GPC measurements: M_n 6.23 kDa, M_w 7.40 kDa, PDI 1.19.

3.5. Polymer **P2**. Polymer **P2** was synthesized following the same procedure as for polymer **P1**. The reaction time was approximately 40 h. Yield: 0.14 g, 0.13 mmol, 86%. ^{1}H NMR (400 MHz, $CDCl_3$, δ (ppm)): 8.99 (br, 2H, Ar-H), 8.83 (br, 2H, Ar-H), 8.05 (br, 2H, Ar-H), 6.84 (1H, thiophene H), 6.75 (1H, thiophene H), 4.20 (br, 4H, -O-CH_2-), 4.20 (br, 6H, -OCH_3), 3.82-3.73 (br, 2H, -N-CH_2-), 1.75-2.02 (br, 6H, -CH_2-), 1.00-1.40 (br, 54H, -CH_2-), 0.70-0.85 (br, 9H, -CH_3). Molecular weights from GPC measurements: M_n 4.40 kDa, M_w 5.09 kDa, PDI 1.16.

Data Availability

Data are included in supplementary information files.

Disclosure

Part of this study is based on Dr. Kuldeep Shetye's dissertation (Shetye, Kuldeep C. "Synthesis, Characterization and Device Studies of Conjugated Foldamers," *Ph.D. Dissertation*, Chemistry and Pharmaceutical Science, University of Missouri-Kansas City, Kansas City, Missouri, USA, 2017).

Conflicts of Interest

The authors declare that they have no conflicts of interest.

Acknowledgments

This work is supported by the National Science Foundation (DMR1308577).

Supplementary Materials

^{1}H NMR spectrum of monomer **M1**. Detailed fluorescence spectra and GPC traces of the polymers. *(Supplementary Materials)*

References

[1] H. Naarmann, "Polymers, electrically conducting," in *Ullmann's Encyclopedia of Industrial Chemistry*, Wiley-VCH, Weinheim, Germany, 2002.

[2] N. K. Elumalai and A. Uddin, "Open circuit voltage of organic solar cells: an in-depth review," *Energy & Environmental Science*, vol. 9, no. 2, pp. 391–410, 2016.

[3] L. Meng, Y. Zhang, X. Wan et al., "Organic and solution-processed tandem solar cells with 17.3% efficiency," *Science*, vol. 361, no. 6407, pp. 1094–1098, 2018.

[4] A. Wadsworth, M. Moser, A. Marks et al., "Critical review of the molecular design progress in non-fullerene electron acceptors towards commercially viable organic solar cells," *Chemical Society Reviews*, vol. 48, no. 6, pp. 1596–1625, 2019.

[5] J. Urieta-Mora, I. García-Benito, A. Molina-Ontoria, and N. Martín, "Hole transporting materials for perovskite solar cells: a chemical approach," *Chemical Society Reviews*, vol. 47, no. 23, pp. 8541–8571, 2018.

[6] T. H. Schloemer, J. A. Christians, J. M. Luther, and A. Sellinger, "Doping strategies for small molecule organic hole-transport materials: impacts on perovskite solar cell performance and stability," *Chemical Science*, vol. 10, no. 7, pp. 1904–1935, 2019.

[7] E. H. Jung, N. J. Jeon, E. Y. Park et al., "Efficient, stable and scalable perovskite solar cells using poly (3-hexylthiophene)," *Nature*, vol. 567, no. 7749, pp. 511–515, 2019.

[8] C. Bizzarri, E. Spuling, D. M. Knoll, D. Volz, and S. Bräse, "Sustainable metal complexes for organic light-emitting diodes (OLEDs)," *Coordination Chemistry Reviews*, vol. 373, pp. 49–82, 2018.

[9] T. Huang, W. Jiang, and L. Duan, "Recent progress in solution processable TADF materials for organic light-emitting diodes," *Journal of Materials Chemistry C*, vol. 6, no. 21, pp. 5577–5596, 2018.

[10] G. Zhan, Z. Liu, Z. Bian, and C. Huang, "Recent advances in organic light-emitting diodes based on pure organic room temperature phosphorescence materials," *Frontiers in Chemistry*, vol. 7, p. 305, 2019.

[11] C. Liu, Y. Xu, and Y.-Y. Noh, "Contact engineering in organic field-effect transistors," *Materials Today*, vol. 18, no. 2, pp. 79–96, 2015.

[12] B. Lüssem, C. M. Keum, D. Kasemann, B. Naab, Z. Bao, and K. Leo, "Doped organic transistors," *Chemical Reviews*, vol. 116, no. 22, pp. 13714–13751, 2016.

[13] H. Li, W. Shi, J. Song et al., "Chemical and biomolecule sensing with organic field-effect transistors," *Chemical Reviews*, vol. 119, no. 1, pp. 3–35, 2019.

[14] Y. Zhang, Y. Yuan, and J. Huang, "Detecting 100 fW cm −2Light with trapped electron gated organic phototransistors," *Advanced Materials*, vol. 29, no. 5, 2017.

[15] C. Qian, J. Sun, L. A. Kong et al., "High-performance organic heterojunction phototransistors based on highly ordered copper phthalocyanine/para-sexiphenyl thin films," *Advanced Functional Materials*, vol. 27, no. 6, 2017.

[16] J. Park, J. H. Seo, S. W. Yeom et al., "Flexible and transparent organic phototransistors on biodegradable cellulose nanofibrillated fiber substrates," *Advanced Optical Materials*, vol. 6, no. 9, 2018.

[17] N. Espinosa, R. G. Valverde, M. S. G. Cascales, and A. Urbina, "Towards low-cost manufacturing of organic solar cells: multi criteria assessment of fabrication technologies," *Renewable Energy and Power Quality Journal*, vol. 1, no. 8, pp. 977–982, 2010.

[18] A. Schöll and F. Schreiber, "thin films of organic molecules," *Molecular Beam Epitaxy*, pp. 591–609, 2013.

[19] Y. Yuan, G. Giri, A. L. Ayzner et al., "Ultra-high mobility transparent organic thin film transistors grown by an off-centre spin-coating method," *Nature Communications*, vol. 5, no. 1, 2014.

[20] G. Giri, E. Verploegen, S. C. B. Mannsfeld et al., "Tuning charge transport in solution-sheared organic semiconductors using lattice strain," *Nature*, vol. 480, no. 7378, pp. 504–508, 2011.

[21] G. R. Llorente, M. B. Dufourg-Madec, D. J. Crouch, R. G. Pritchard, S. Ogier, and S. G. Yeates, "High performance, acene-based organic thin film transistors," *Chemical Communications*, no. 21, pp. 3059–3061, 2009.

[22] J. G. Laquindanum, H. E. Katz, and A. J. Lovinger, "Synthesis, morphology, and field-effect mobility of anthradithiophenes," *Journal of the American Chemical Society*, vol. 120, no. 4, pp. 664–672, 1998.

[23] M. M. Payne, S. R. Parkin, J. E. Anthony, C. C. Kuo, and T. N. Jackson, "Organic field-effect transistors from solution-deposited functionalized acenes with mobilities as high as 1 $cm^2/V{\cdot}s$," *Journal of the American Chemical Society*, vol. 127, no. 14, pp. 4986-4987, 2005.

[24] Y. Mei, M. A. Loth, M. Payne et al., "High mobility field-effect transistors with versatile processing from a small-molecule organic semiconductor," *Advanced Materials*, vol. 25, no. 31, pp. 4352–4357, 2013.

[25] H. Ebata, T. Izawa, E. Miyazaki et al., "Highly soluble [1]benzothieno[3,2-b]benzothiophene (BTBT) derivatives for high-performance, solution-processed organic field-effect transistors," *Journal of the American Chemical Society*, vol. 129, no. 51, pp. 15732-15733, 2007.

[26] T. Uemura, Y. Hirose, M. Uno, K. Takimiya, and J. Takeya, "Very high mobility in solution-processed organic thin-film transistors of highly ordered [1]benzothieno[3,2-b]benzothiophene derivatives," *Applied Physics Express*, vol. 2, no. 11, article 111501, 2009.

[27] C. Liu, T. Minari, X. Lu, A. Kumatani, K. Takimiya, and K. Tsukagoshi, "Solution-processable organic single crystals with bandlike transport in field-effect transistors," *Advanced Materials*, vol. 23, no. 4, pp. 523–526, 2011.

[28] Y. S. Yang, T. Yasuda, H. Kakizoe et al., "High performance organic field-effect transistors based on single-crystal microribbons and microsheets of solution-processed dithieno[3,2-b:2′,3′-d]thiophene derivatives," *Chemical Communications*, vol. 49, no. 58, pp. 6483–6485, 2013.

[29] S. K. Park, T. N. Jackson, J. E. Anthony, and D. A. Mourey, "High mobility solution processed 6,13-bis(triisopropyl-silylethynyl) pentacene organic thin film transistors," *Applied Physics Letters*, vol. 91, no. 6, article 063514, 2007.

[30] Y. Li, T. Dutta, N. Gerasimchuk et al., "Conjugated foldamers with unusually high space-charge-limited current hole mobilities," *ACS Applied Materials & Interfaces*, vol. 7, no. 18, pp. 9372–9384, 2015.

[31] Y. Li, R. G. Clevenger, L. Jin, K. V. Kilway, and Z. Peng, "Unusually high SCLC hole mobility in solution-processed thin films of a polycyclic thiophene-based small-molecule semiconductor," *Journal of Materials Chemistry C*, vol. 2, no. 35, pp. 7180–7183, 2014.

[32] Y. Li, R. G. Clevenger, L. Jin, K. V. Kilway, and Z. Peng, "Spin-coated thin films of polycyclic aromatic hydrocarbons exhibiting high SCLC hole mobilities," *Journal of Physical Chemistry C*, vol. 120, no. 2, pp. 841–852, 2016.

[33] Y. Li, K. R. Scheel, R. G. Clevenger et al., "Highly efficient and stable perovskite solar cells using a dopant-free inexpensive small molecule as the hole-transporting material," *Advanced Energy Materials*, vol. 8, no. 23, 2018.

[34] B. R. Kaafarani, "Discotic liquid crystals for opto-electronic applications," *Chemistry of Materials*, vol. 23, no. 3, pp. 378–396, 2011.

[35] H. K. Bisoyi and Q. Li, "Light-driven liquid crystalline materials: from photo-induced phase transitions and property modulations to applications," *Chemical Reviews*, vol. 116, no. 24, pp. 15089–15166, 2016.

[36] K. Goossens, K. Lava, C. W. Bielawski, and K. Binnemans, "Ionic liquid crystals: versatile materials," *Chemical Reviews*, vol. 116, no. 8, pp. 4643–4807, 2016.

[37] T. Wöhrle, I. Wurzbach, J. Kirres et al., "Discotic liquid crystals," *Chemical Reviews*, vol. 116, no. 3, pp. 1139–1241, 2016.

[38] H. Ito, Y. Segawa, K. Murakami, and K. Itami, "Polycyclic arene synthesis by annulative π-extension," *Journal of the American Chemical Society*, vol. 141, no. 1, pp. 3–10, 2018.

[39] J. Kim, D. T. McQuade, A. Rose, Z. Zhu, and T. M. Swager, "Directing energy transfer within conjugated polymer thin films," *Journal of the American Chemical Society*, vol. 123, no. 46, pp. 11488-11489, 2001.

[40] A. Rose, C. G. Lugmair, and T. M. Swager, "Excited-state lifetime modulation in triphenylene-based conjugated polymers," *Journal of the American Chemical Society*, vol. 123, no. 45, pp. 11298-11299, 2001.

[41] C.-E. Chou, D. Wang, M. Bagui, J. Hsu, S. Chakraborty, and Z. Peng, "Syntheses and optical properties of triphenylene-containing conjugated polymers," *Journal of Luminescence*, vol. 130, no. 6, pp. 986–994, 2010.

[42] M. Bagui, J. S. Melinger, S. Chakraborty, J. A. Keightley, and Z. Peng, "Synthesis and optical properties of triphenylene-based conjugated dendrons," *Tetrahedron*, vol. 65, no. 7, pp. 1247–1256, 2009.

[43] D. Wang, J. F. Hsu, M. Bagui et al., "Synthesis and self-assembly of a triphenylene-containing amphiphilic conjugated macrocycle," *Tetrahedron Letters*, vol. 50, no. 18, pp. 2147–2149, 2009.

[44] H. Xin, X. Guo, F. S. Kim, G. Ren, M. D. Watson, and S. A. Jenekhe, "Efficient solar cells based on a new phthalimide-based donor–acceptor copolymer semiconductor: morphology, charge-transport, and photovoltaic properties," *Journal of Materials Chemistry*, vol. 19, no. 30, pp. 5303–5310, 2009.

[45] T. Dutta, Y. Li, A. L. Thornton, D. M. Zhu, and Z. Peng, "Imide-functionalized naphthodithiophene based donor-acceptor conjugated polymers for solar cells," *Journal of Polymer Science Part A: Polymer Chemistry*, vol. 51, no. 18, pp. 3818–3828, 2013.

[46] J. Duan, L. H. Zhang, and W. R. Dolbier, Jr, "A convenient new method for the bromination of deactivated aromatic compounds," *Synlett*, vol. 1999, no. 8, pp. 1245-1246, 1999.